SAND79-2339
Unlimited Release
UC-20b

Compressed Magnetic Flux With Capacitive Load

Otmar M. Stuetzer

Sandia National Laboratories

SAND79-2339
Unlimited Release
Printed March 1980

Distribution
Category UC-20b

COMPRESSED MAGNETIC FLUX AMPLIFIER WITH CAPACITIVE LOAD

Otmar M. Stuetzer
Energy Subsystems Division 2165
Sandia Laboratories
Albuquerque, NM 87185

ABSTRACT

A first-order analysis is presented for a compressed magnetic flux (CMF) current amplifier working into a load with a capacitive component. Since the purpose of the investigation was to gain a general understanding of the arrangement, a number of approximations and limitations were accepted. The inductance of the transducer varies with time; the inductance/resistance/ capacitance (LRC) circuit therefore is parametric and solutions are different for the stable regime (high C), the oscillation regime (low C), and the transition case. Solutions and performance depend strongly on circuit boundary conditions, i.e., energization of the circuit by either an injected current or by an applied capacitor charge. The behavior of current and energy amplification for the various cases are discussed in detail. A number of experiments with small CMF devices showed that the first-order theory presented predicts transducer performance well in the linear regime.

ACKNOWLEDGMENT

The work was performed at the suggestion of J. E. Gover. J. L. Johnson prepared the experiments. E. C. Cnare and T. J. Tucker contributed greatly to data evaluation. P. C. Reardon of Science Applications, Inc., checked our analytic solutions by means of a computer program.

CONTENTS

ILLUSTRATIONS

ILLUSTRATIONS (cont)

TABLES

COMPRESSED MAGNETIC FLUX AMPLIFIER WITH CAPACITIVE LOAD

Introduction

This investigation is based on preceding work analyzing the operation of a compressed magnetic flux (CMF) transducer into an inductive-resistive load.[1] A second-order theory for this combination[2] takes into account the variation of skin depth with time, and flux trapping by wire shape and by two contact delay phenomena. An attempt to extend this second-order theory directly to the capacitive load case proved analytically unfeasible. We will use the analysis of Ref 2 only to determine the rather sensitive end values of generator inductance and generator resistance; inductance and resistance will then be approximated quite accurately by a parabolic function and by a linear function, respectively. A second-order differential equation results which, for the general case, has to be computer-integrated. However, if we limit one resistance or one inductance parameter to specific values determined by the other parameters a very simple analytic solution results, which we shall pursue. The load resistance was selected as the limited parameter for the derivation; it may be replaced by other resistances or inductances. The limitation introduced is not a severe one for practical cases.

Inductances and Resistances

As Figure 1 illustrates, our arrangement is a series circuit of inductances (L), resistances (R), and the load capacitance (C). The inductance and resistance of the generator coil are shorted out progressively, but not completely, by the explosively expanding armature. From Ref 1 we know that the inductance at crowbar time, $t = 0$, is the sum of the coil inductance L_o and the load inductance L_L. At end of compression, $t = t_c$, the inductance has an end value L_e, which is the sum of load inductance L_L and a remnant inductance L_R. The decrease from initial to end inductance is nearly parabolic. Similarly, we have during compression a decrease of device resistance from $R_o + R_L$ to an end resistance R_e; this decrease is linear, however.

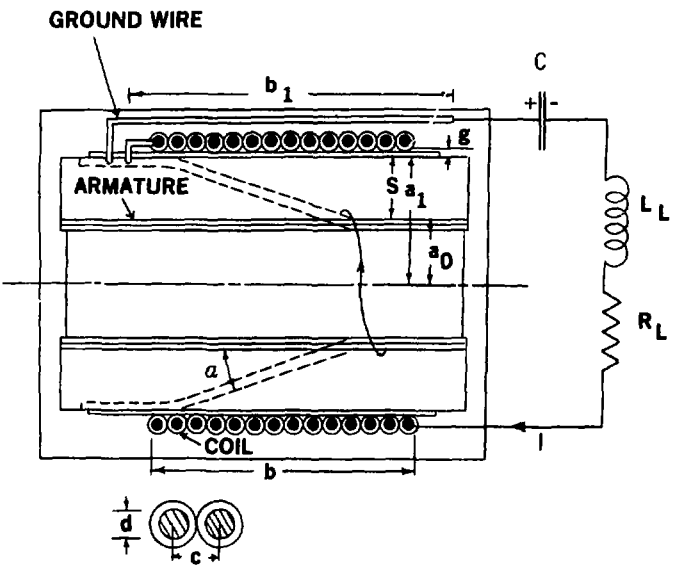

Figure 1. Schematic of Transducer and Load

From Eqs (14) and (11) of Ref. 1 we obtain the following values for L_e and R_e:

$$L_e = L_o \cdot k\sqrt{\frac{8}{R_m}}\,(1-\Gamma)\left\{\tau^* + \frac{(1-\Gamma)^2}{12}\right\} + L_L \qquad (1a)$$

$$R_e = R_o \cdot \frac{1}{1-\Gamma}\left\{\tau^* + \frac{(1-\Gamma)^2}{12}\right\} + R_L \quad . \qquad (1b)$$

Here k is a wire shape factor close to unity, R_m is the magnetic Reynolds number for the flux compressor, Γ is the slope of the time decrease of the skin layer thickness and has values between 0.4 and 0.6, and τ^* is the insulator breakdown delay time normalized to the compression time t_c and is of the order of magnitude 0.03. All these quantities are discussed in Refs. 1 and 2 in much more detail. In practice, L_e and R_e, and with them L_L and R_L, are much smaller than the initial values L_o and R_o.

With this, the time functions for inductance and resistance, which show the proper initial values and end values, can be written:

$$L(t) = \left(L_o + L_L\right)\left[1 - \frac{t}{t_c}\left(1-\sqrt{\frac{L_e}{L_o + L_L}}\right)\right]^2 \qquad (2a)$$

$$R(t) = \left(R_o + R_L\right)\left[1 - \frac{t}{t_c}\left(1-\frac{R_e}{R_o + R_L}\right)\right] \qquad (2b)$$

for times $0 \le t \le t_c$.

We now make the time parameters for the two equations identical by stipulating

$$\sqrt{\frac{L_e}{L_o + L_L}} = \frac{R_e}{R_o + R_L} \qquad (3)$$

or, in practical cases, limiting the load resistance R_e to $R_e = R_o\sqrt{L_e/L_o}$. Equation (3) together with Eq (2) selects a value for R_L, or R_o, at our option.

Abbreviating: $L_o + L_L = L_1$ (4)

$$R_o + R_L = R_1 ,$$

and introducing a time parameter X and a compression parameter α by writing

$$X = 1 - \alpha \frac{t}{t_c} \tag{5}$$

$$\alpha = 1 - \sqrt{\frac{L_e}{L_o + L_L}} ,$$

we can now conveniently write for the time functions:

$$L(t) = L_1 X^2 , \tag{6a}$$

$$R(t) = R_1 X , \tag{6b}$$

$$1 \geq X \geq 1 - \alpha .$$

The physical meaning of our mathematical manipulations is that we have defined a new compressor coil, longer by a factor of about $1/\alpha$, the entire length of which we do not completely use. This way, the proper inductance L_e and resistance R_e stay in the circuit.

The Circuit Equation

All the voltages in the circuit of Figure 1 must add up to the voltage U_o originally applied across the capacitor C (if any); thus, we have for the current I in the transducer

$$\frac{d}{dt} (L I) + RI + \frac{1}{C}\int I \, dt = U_o .$$

We introduce the flux linkage $\phi = LI$ and differentiate:

$$\frac{d^2}{dt^2}\phi + \frac{d}{dt}\left(\frac{R}{L}\phi\right) + \frac{1}{LC}\phi = 0 \quad . \tag{7}$$

For practical use we will consider two boundary conditions for circuit Eq (7):

1. At time $t = 0$, an injected current I_o flows in the system but there is no voltage across the capacitor ($U_o = 0$)
2. At time $t = 0$, a voltage U_o exists over the capacitor C but no current is flowing ($I_o = 0$).

We change the variable t to the variable X of Eq (5), with $dX = -(\alpha/t_c)\,dt$, and introduce the values for R and L from Eq (6). With the prime representing differentiation after X, we obtain

$$X^2\phi'' - \frac{R_1 t_c}{\alpha L_1} X\phi' + \left(\frac{R_1 t_c}{\alpha L_1} + \frac{t_c^2}{2\alpha L_1 C}\right)\phi = 0 \quad . \tag{8}$$

This is an Euler equation, and the solutions are readily available in the literature.[3] The two arbitrary constants occurring in the solution of a second order differential equation have to be determined from the boundary conditions (1 or 2) above. The algebra for this determination, while straightforward, is quite lengthy and will not be detailed here.

To allow the solution to be expressed conveniently, we shall define a number of abbreviations in Table 1, which also contains a repetition of former essential definitions.

Table 1

Definitions

I	Current
U	Voltage across capacitor
L_o	Inductance of coil (at crowbar)
L_e	End inductance (see Eq 2), $\ll L_o$
	L_L/L_o, $\ll 1$
	$1 - \sqrt{L_e/(L_o + L_L)}$, compression factor, ~ 1
U_o	Applied capacitor voltage
I_o	Injection current
I^*	$(U_o/L_o)\ (t_c/\alpha)/(1 + \ell)$ } reference quantities
U^*	$I_o.L_o(\alpha/t_c)\ (1 + \ell)$ } reference quantities
X	$1 - \alpha\ t/t_c$, time parameter
ω^2	$(L_oC)^{-1}\ (1 + \ell)^{-1}$, basic angular frequency
$-\gamma$	$1/2 + R_o\ t_c/\left[(1 + \ell).\ 2\ L_o\alpha^2\right]$,
	Damping constant $\approx -1/2$
β^2	$\left\lvert\gamma^2 - \omega^2 t_c^2/\alpha^2\right\rvert$; oscillation parameter

Solutions

The solutions for circuit current I and capacitor voltage U, normalized to the appropriate circuit dependent constants from Table 1, are listed in Table 2. The dominant factors are $x^{-\gamma}$ for the voltage rise with time and $x^{-\gamma-1}$ for the current rise with time t. For low

circuits, these factors behave as

$$1/\sqrt{1 - \alpha t/t_c} \qquad \text{or} \qquad 1/\sqrt{1 - \alpha t/t_c}^{\,3} \quad ,$$

respectively. At end of compression, $t \rightarrow t_c$, the values increase rapidly. The equations are not valid for $t > t_c$.

Table 2

Solutions for Circuit Current I and Capacitor Voltage U

	STABLE CASE A $\gamma > \omega t_c/\sigma$	TRANSITION CASE B $\gamma = \omega t_c/\sigma$	OSCILLATORY CASE C $\gamma < t_c/\sigma$	U
(a) Injected Current I_o				
$\frac{I}{I_o} =$	$X^{-\gamma-1}\begin{bmatrix} X^{\beta} + X^{-\beta} \\ -\frac{\gamma}{\beta}\left(X^{\beta} - X^{-\beta}\right) \end{bmatrix}$	$X^{-\gamma-1}\left[1 - \gamma\ \ell n\ X\right]$	$X^{-\gamma-1}\begin{bmatrix} \cos\left(\beta\ \ell n\ X\right) \\ -\frac{\gamma}{\beta}\sin\left(\beta\ \ell n\ X\right) \end{bmatrix}$	T2-1
$\frac{U}{U^*} =$	$\frac{X^{-\gamma}}{2}\ \frac{2t_c}{\alpha^2\beta}^2\left[X^{\beta} - X^{-\beta}\right]$	$X^{-\gamma} \cdot \gamma^2\ \ell n\ X$	$X^{-\gamma}\ \frac{2t_c}{\alpha^2\beta}^2\ \sin\left(\beta\ \ell n\ X\right)$	T2-2
(b) Applied Voltage U_o				
$\frac{I}{I^*} =$	$\frac{X^{-\gamma-1}}{2}\ \frac{1}{\beta}\left[X^{\beta} - X^{-\beta}\right]$	$X^{-\gamma-1}\ \ell n\ X$	$X^{-\gamma-1} \cdot \frac{1}{\beta}\ \sin\left(\beta\ \ell n\ X\right)$	T2-3
$\frac{U}{U_o} =$	$\frac{X^{-\gamma}}{2}\begin{bmatrix} X^{\beta} + X^{-\beta} \\ \frac{\gamma}{\beta}\left(X^{\beta} - X^{-\beta}\right) \end{bmatrix}$	$X^{-\gamma}\left[1 + \gamma\ \ell n\ X\right]$	$X^{-\gamma}\begin{bmatrix} \cos\left(\beta\ \ell n\ X\right) \\ \frac{\gamma}{\beta}\ \sin\left(\beta\ \ell n\ X\right) \end{bmatrix}$	T2-4

For very high capacitances and low resistances, the current rises approximately as x^{-2}. This follows from Eq T2-1 Case A, in Table 2 for $C \to \infty$, or $\beta \to \gamma$, as well as from direct integration of the now simple Eq (7). With decreasing values of C, the current rise becomes more like $x^{-3/2}$. The device is stable.

Decrease of the capacitance C leads to the boundary of the stability region. The transition case is characterized by $\omega t_c = \gamma\alpha$, or a transition capacitance

$$C_t = \frac{t_c^2}{\alpha^2\left(L_o + L_L\right)\left[\frac{1}{2} - \frac{R_o t_c}{2 L_o} \cdot \frac{1}{(1+\ell)} \cdot \frac{1}{\alpha^2}\right]^2} \quad . \tag{9}$$

For low resistance we have $C_t \approx 4t_c^2/L_o$.

In Figure 2 solutions for the transition case (Table 2, B) have been plotted for a set of parameters occurring in practice. The abscissa is the normalized compression time, t/t_c. For current injection (Case a), the current rises to about 40 times the original value I_o; a (negative) voltage builds up on the capacitor, first linearly, then faster. For initiation by applied voltage U_o (Case b), the voltage drops to about two-thirds, while a first slowly, then fast rising current builds up in the circuit.

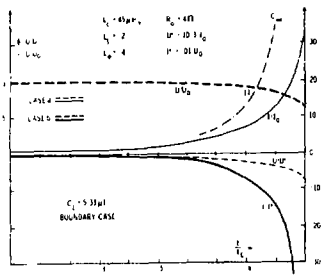

Figure 2. Time Dependence of Normalized Current and Voltage for Transition Capacitance C_t

If C is larger than the critical value C_t, current changes are higher in absolute values, voltage changes are lower. For infinitely large C, (and $R_o = 0$), the maximum possible current increase results; it is indicated in Figure 2. U is identically zero in this case, of course. The critical capacitance C_t decreases with decreasing losses according to Eq. (9).

When C becomes smaller than C_t, currents and voltages start reversing during compression; finally, oscillations develop. An example is shown in Figure 3 for a capacitance of about 1/100 of C_t, and for Case b, energization through capacitor charging. Current and voltage drop into a phase shift of $\pi/2$: whenever one has an extreme value, the other one reverses.

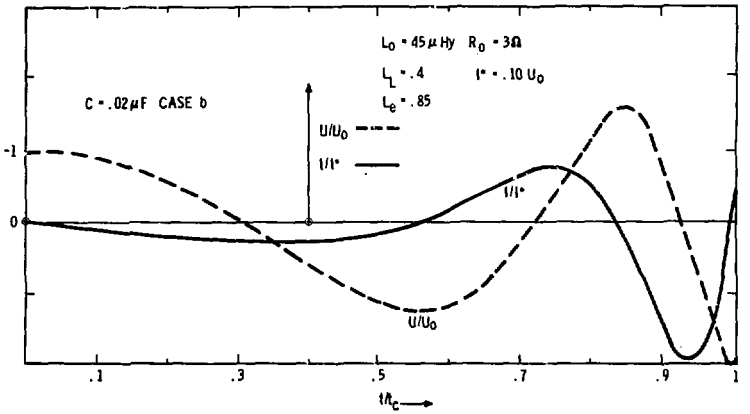

Figure 3. Example of Oscillatory Response for Capacitor Charge-Up Initiation

In Figure 4 the capacitance is decreased by another factor of 10: more oscillation periods are in evidence. (Their number is proportional

to $1/\sqrt{C}$, but depends somewhat on the loss resistance R_o). We see that the voltage maxima have about the same value as in Figure 3. The current is decreased, however, as the lower capacitance means a higher circuit impedance. The voltage swings increase slightly towards the end of compression, indicating an increase in the energy ($CU^2/2$). This energy amplification is due to our assumption of $R_o = 3\Omega$. For $R = 12\Omega$, the voltage extrema would decrease markedly towards the end. R has little influence on the time position of the maxima or zeros.

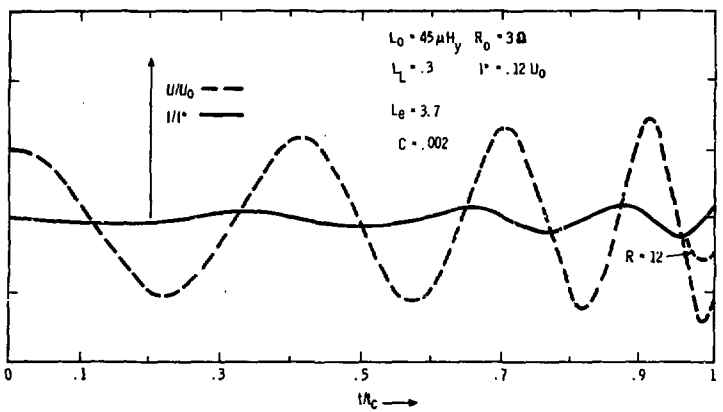

Figure 4. Circuit Behavior for Capacitance Decreased by Factor 10 With Respect to Figure 3

The periods of the output decrease towards the end of compression as the inductance decreases. The device delivers a "chirp pulse". Increase of the load inductance L_L moves the time curves to the right, as expected. After $t = t_c$, no additional energy is furnished to the circuit. It rings out, first with inductance L_e, and after a time $\tau * t_c$ with inductance L_L.

If the mathematically simplifying condition (3) is dropped, R_L enters the analysis as an additional free parameter. Circuit Eq (7) becomes a second order hypergeometric differential equation which can only be computer integrated. P. C. Reardon has performed the integration.[4] The deviations from our approximation are small for factors of 2 or 3 in R_L.

Our solution is therefore certainly very suitable for a general assessment of device behavior.

Discussion

The capacitively loaded CMF amplifier will now be discussed more generally with the help of Figure 5 in which the end amplification ratios (i.e., the values predicted analytically from Table 2) at time t_c are plotted vs decreasing capacitance C for L_o = 65 μHy, L_L = 0.3, L_e = 0.6, and R_o = 3μ. The normalization parameters for this case have the values U^* = 14.8 I_o and I^* = 0.07 U_o. The transition capacitance C_t = 2 μF is indicated in the graph (lower left side).

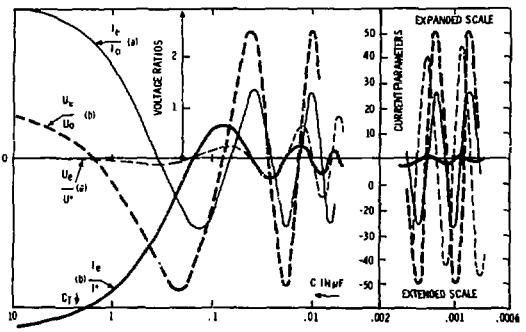

Figure 5. Normalized Voltage and Current Values at End of Compression ($t = t_c$) for Current Injection (thin curves) and for Voltage Initiation (thick curves)

We see that at the end of compression, currents and voltages fluctuate between maxima and minima, as is to be expected for a family of oscillating circuits. There is a 90° phase shift between them; this is a direct effect of the 90° shift on the time axis discussed above.

Case a: for injected currents I_o, the end currents reach quite high values for large load capacitances C (Regime A, Figure 5). In the oscillating regime, the current maxima and minima are lower and independent of C. The maximum voltages increase with decreasing C.

Case b: for initiation of the system by a voltage U_o (or charge CU_o), the end voltage after compression will be smaller than U_o in Regime A. In the oscillating regime, the voltage extremes are independent of C, and, in our example, about 2.5 times the applied voltage. The current maxima decrease with decreasing C.

This somewhat involved behavior becomes understandable, if we look at the energy amplification η of the transducer. At $t = o$, the energy furnished is $(L_o + L_L)\, I_o{}^2/2$ for injected currents and $CU_o{}^2/2$ for voltage initiation. The output energy at $t = t_c$ is partly stored in the load inductance L_e and partly in the capacitance C. The part stored in the nonload portion of the end inductance L_e (first form of Eq (1a)) is inaccessible to us but will be considered here. For injected currents the output energy is

$$L_e I_e{}^2/2 + CU_e{}^2/2 = L_e\,(I_e/I_o)^2 I_o{}^2/2 + C\,(U_e/U^*)^2 \cdot U^{*2}/2 \quad ;$$

replacing U^* from Table 1, we find

$$\eta_a = \frac{L_e}{L_o + L_L} \cdot \left(\frac{I_e}{I_o}\right)^2 + \frac{\alpha^2}{t_c{}^2} \left(L_o + L_L\right) C \left(\frac{U_e}{U^*}\right)^2 . \qquad (10a)$$

Similary, for injected currents:

$$\eta_b = \frac{t_c{}^2}{\alpha^2} \frac{I_e}{L_o + L_L} \cdot \frac{1}{C} \left(\frac{I_e}{I^*}\right)^2 + \frac{U_e{}^2}{U_o{}^2} \quad . \qquad (10b)$$

Oscillating Regime

Taking the values of I_e/I_o, U_e/U^*, etc, from Figure 5, and inserting them into Eq (10), we find that within our approximation $_a$ and $_b$ are about equal and about constant. This is not surprising; circuits with relatively low losses should behave that way after a number of cycles. The energy, while building up, fluctuates from inductance to capacitance and back. If we look now at the capacitor values where I_e/I_o is zero, i.e., all end energy is in the capacitor, the product $C\,(U_e/U^*)^2$ should be constant; the maxima and minima of U_e should therefore vary with $1/\sqrt{C}$. Correspondingly, for injected currents the quotient $(I_e/I^*)^2/C$ should be constant for the current maxima, which then will vary as $\sqrt{C}$. Figure 5 shows that both conclusions are approximately correct.

In the oscillating regime, the values for energy amplification η_a and η_b are about 6.25 for the case plotted in Figure 5, where a resistance $R_o = 3\Omega$ was chosen. For better transducers, if they can be produced, higher amplifications are predicted. (If R_o were 1Ω in Figure 5, we would expect a nine-fold energy gain.)

Stable Regime

Figure 5 shows clearly, that for current injection, the current amplification is larger by about a factor 2 than the maximum current amplification in the oscillating regime. According to Eq (10a), the energy gain is therefore much larger. For very high capacitance C, the current amplifications approach those for a purely inductive-resistive system, as treated in Ref. 1. Energy amplification, therefore, decreases from stable to oscillating regime. The main reason for this is that current and therefore magnetic field reverse during compression (Figure 3). While the field is in the neighborhood of zero, the mechano-magnetic transduction mechanism does not operate. A contributing factor is that in certain configurations, due to faster time variations, the skin effect losses rise.

For initiation by a capacitor voltage, the amplification in the stable regime is lower than for the oscillating regime (Figure 5). This is due to the fact that the magnetic field starts at zero at the beginning of compression and is being established quite gradually (Figure 2). For large capacitances the capacitor still holds energy at $t = t_c$, which would be needed to generate the magnetic working field.

Comments on Applications

The preceding discussion described the physics of the device. For actual applications, a number of additional points must be considered.

It was evident from our derivation that we cannot take energy out of the total inductance L_e; only the load part L_L is accessible to us. This seems to make energy from capacitive storage in C preferable, but in practice, every capacitor has a series inductance and what is accessible *is always an LRC combination. This reduces the energy gain.*

It may appear from the above discussion that from the energy gain point of view, the voltage U_o initiated arrangement is inferior; in the oscillating regime it is not better than the injection current initiated transducer, and in the high C regime it is much worse. Actually, by introduction of a switch voltage initiation can be transformed into injected current: we charge up the capacitor, short the circuit, and after a quarter period of oscillation there will be maximum current in the coil and no voltage across the capacitor. At this moment we start field compression.

Experiments

Nine experiments were performed with laboratory test unit (LTU) transducers described in Ref. 1. The aggravating problems caused by insufficiently precise machining of coils, armatures, and explosive

sticks discussed in Ref. 1 were in full evidence. Considerable data scatter and an occasional discontinuity had to be accepted.

All shots were performed with capacitor charge initiation, which is experimentally much simpler than current injection.

Parameter Values

The effective measuring circuit is shown in Figure 6. Inductance L_C and resistance R_C of the capacitor package C is not negligible in our experiments. L_M and R_M are values belonging to the measurement circuit and the CVT current gauge, and are of the order 50 nH and 30 mΩ, respectively. L_R and R_R are the inductance and resistance remaining in the coil at end of compression; according to Ref. 1 we expect contributions of about 0.4 μH and 36 mΩ.

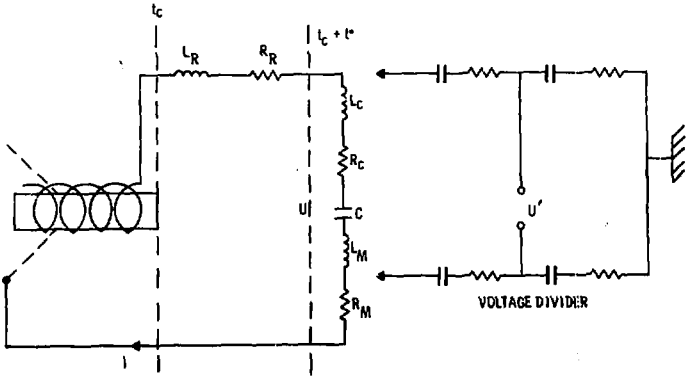

Figure 6. Measuring Arrangement With Location of Short Circuit at Time t_c and at Time $t_c + t^*$

The circuit rings out after the end of compression; this will be more fully discussed later. The ringing frequency is first determined by C and all the inductances and resistances still in the circuit after compression. After a time t^*, about 200 μs in our case, L_R and R_R have disappeared and the circuit assumes a somewhat higher frequency. For small L_L, the effect is well observable and is a direct proof of the

existence of L_R, the remanent inductance. The ring-out gives us the opportunity to determine inductances and resistances in the circuit by measuring frequency and decrement. In practice, this is reasonably accurate only for the end of the ringout, permitting us to measure $L_L = L_C + L_M$ and $R_L = R_C + R_M$. The end-compression values L_e and R_e can then be determined by adding L_R and R_R from reference 1, or by using Eq (1).

The initial inductance L_o at crowbar was 45 H for the experimental transducers. This gives us $L_1 = L_o + L_L$, which we need for determining the parameters in Table 1.

We have determined R_e experimentally, so the initial circuit resistance $R_o + R_L$ is no longer free but is determined by Eq (3). This causes errors at the beginning of compression but guarantees proper parameter values at the end, where it is important.

The capacitances used and the inductances and resistances determined as described are listed in the left column of Table 3. With them, and Table 1, we can check our theory, using the equations of Table 2.

Current Measurements

Current vs time, predicted by Eq (3) of Table 1, was measured by a calibrated current viewing transformer. Excellent agreement was found both for shape and amplitude.

As an example, Figure 7 shows the current trace for Shot 2 (see Table 3) as plotted by computer from digitized data. The load capacitor was 0.02 F. Except for sign reversal, the shape of the curve is the one predicted by Figure 3 (for a slightly different starting resistance). Peak values are well within 10% of prediction.

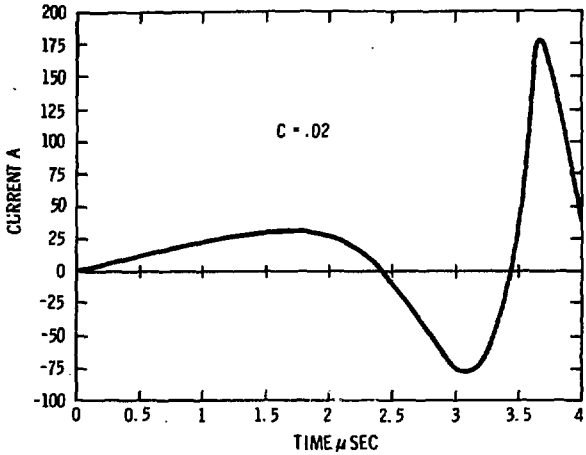

Figure 7. Shot 2, Computer Retrieved Digitized Data (C = 0.02 μF)

Table 3

Expected and Measured Currents

C	L_L	L_e	L_1	R_L	R_e	R_1	Shot No.	Max. Current I_{exp}	Max. Current $I_{Meas.}$	$\frac{L_1 I^2}{CU_o^2}$
2	0.75	1.15	45.8	0.35	0.71	4.5	8	1730	1760	1.2
							9	1730	1650	1.1
0.02	0.43	0.83	45.4	0.28	0.64	4.7	1	167	151	0.5
							2	167	181	0.7
0.002 (High L_L)	3.2	3.61	48.2	2.1	2.5	7.8	3	23	26	1.1
							7	23	24	1.0
0.0025 (Low L_L)	0.38	0.78	45.4	0.48	0.84	6.4	4	76	70	0.75
							5,6	FAILURES		-
μF	μHenries			Ohms				Amps		

$L_{coil} = 45$ H; $L_L = L_{CAP} + L_{CIRCUIT}$; $L_R = 0.40$ H

$R_L = R_{CAP} + R_{CIRCUIT}$; $R_R = 0.36$

$R_1/R_e = L_1/L_e$

A current measurement for a smaller capacitive load C = 0.002 μF, (Shot 7) is plotted in Figure 8 on an extended time scale. The compression time t_c = 4.1 μs is indicated. We see that current is flowing before the device crowbars. This phenomenon is related to preamplification as discussed in Ref. 2. Before crowbar, the coil-armature combination is a capacitance c' charged to voltage U_o. As the armature expands, the capacitance c' decreases, inducing a current U_o dc'/dt into the parametric system and causing preringing.

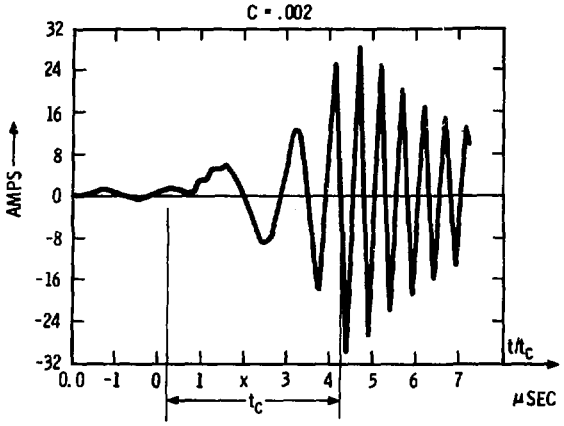

Figure 8. Shot 7, Computer Retrieved Digitized Data

During the first cycle of compression we notice clocking. After compression the circuit rings out, as discussed. We observe a relatively fast decay, due to the high resistance (> 2 Ω) remaining in the circuit. The first cycle is about 6% longer than the subsequent ones due to the presence of the inductance L_R during this time; this agrees with the theoretically predicted percentage $L_R/2L_L$.

Expcted and measured currents for our experiments are listed in Table 3.

Voltage Measurements

Attempts to measure the voltage across the capacitor with a frequency independent, extremely high impedance voltage divider (Figure 6) ran into difficulties. The theory predicts the voltage on the capacitor; what we can measure is the value across the combination L_C, R_C, and C. Circuit analysis demands a correction factor

$$U'/U = \sqrt{(1 - \omega^2 L_C C)^2 + \omega^2 R_C{}^2 C^2} \quad , \tag{11}$$

where ω is the angular ringing frequency and the whole factor is typically between 0.7 and 0.9. This correction factor was not enough for higher frequency devices: there are additional parallel capacitances and series inductances in the circuit which complicate the situation. Occasional breakdown and charge shifts occurred in the voltage measuring circuit. Otherwise, the measurements showed the expected features.

The current measurements were very good, so the voltage across C could be determined by computer integration from I:

$$U - U_o = \left(\int I dt \right) / C.$$

Excellent agreement with theoretical predictions was obtained by this method. An example is shown for Shot 2 in Figure 9, where the current values of Figure 7 were used. We see that the result compares very well with the voltage curve predicted in Figure 3.

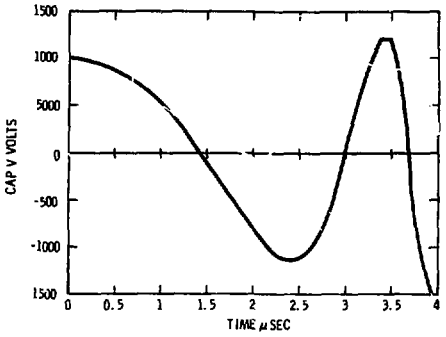

Figure 9. Shot 2, Voltage Across Capacitor Taken From Integrated Current Data

Clocking Resonance

Shots 5 and 6 are marked as failures in Table 3. For these shots, a low inductance load capacitor was chosen. It developed that the capacitor resonance was very close to the clocking frequency. Strong oscillations, high current and voltage amplitudes, and current/voltage jumps occurred. In retrospect, it was recognized that the circuit behavior had to be very complex. While this effect was not pursued further, it could be useful for generation of very high frequencies (20 to 50 MHz) at good power amplification.

Energy Amplification

For the reported experiments the energy amplification was rarely above 1.1 to 1.2, and often below unity. In Table 3, last column, we compare the end energy occurring at maximum current in the inductive part of the load L_L, which is $(L_L I^2)/2$, to the invested energy $(CU_o^2)/2$. For the energy stored in the capacitor, very similar results are obtained. The low values are due to the high resistences and load inductences in our experimental series, and do not signify that the system is useless for energy amplification. It means, however, that for many applications the load will have to be designed carefully.

Conclusion

The analysis presented describes the linear operation of a compressed magnetic flux energy transducer into a general LRC load. A number of approximations and simplifications had to be used. The resistance of the system is taken to vary linearly with time after crowbar, and inductance is described by a parabolic time function (Eq (1)). Considerable inductance and resistance remain in the coil-armature system after compression ends, as analyzed in previous work. Corrections for insulator breakdown delay, field inertia, and skin depth influence are contained in the end values (Eq (1)).

Analysis was found to be feasible only if resistances and inductances are limited by a mutual relationship (Eq (3)). This limitation does not strongly effect the results, especially if the important values at the end of compression are correctly preserved; we did this for our experiments.

Solution of the circuit equation for our parametric circuit distinguishes three cases, a stable regime A, an oscillating regime C, and a transition case B (see Table 3). The solutions are different for different methods of energization: injected current and charged up load capacitor.

A number of experiments with available test units proved that the theory presented describes the arrangement well. We therefore have a basis to analyze device performance for specific applications.

References

[1]J. E. Gover, O. M. Stuetzer, and J. L. Johnson, Small Helical Flux Compression Amplifiers, Proceedings of Second International Conference on Megagaus Fields (1979). In print.

[2]O. M. Stuetzer, "Theory of Small Helical Magnetic Flux Compression Amplifiers," SAND79-1075 (Albuquerque: Sandia Laboratories, Sept 1979).

[3]E. Kamke, Differential Equations, Akademische Verlagsgesellschaft, Leipzig, 194a, p 341.

[4]P. C. Reardon, Coil CMF Generators with an LRC Load, Internal Report, 1120 3rd NW, Albuquerque, NM (Science Applications, Inc., August 1979).